Preserving Symmetry in Convection-Diffusion Schemes

Verstappen, R.W.C.P.; Veldman, A.E.P.

Published in:
Turbulent Flow Computation

Chapter 3

PRESERVING SYMMETRY IN CONVECTION-DIFFUSION SCHEMES

R.W.C.P. Verstappen
verstappen@math.rug.nl

A.E.P. Veldman
Research Institute for Mathematics and Computing Science, University of Groningen
P.O.Box 800, 9700 AV Groningen, The Netherlands.
veldman@math.rug.nl

Abstract We propose to perform turbulent flow simulations in such manner that the difference operators do have the same symmetry properties as the corresponding differential operators. That is, the convective operator is represented by a skew-symmetric difference operator and the diffusive operator is approximated by a

operators forms in itself a motivation for discretizing them in a certain manner. We give it a concrete form by noting that a symmetry-preserving discretization of the Navier-Stokes equations is conservative, *i.e.* it conserves the (total) mass, momentum and kinetic energy (when the physical dissipation is turned off); a symmetry-preserving discretization of the Navier-Stokes equations is stable on any grid. Because the numerical scheme is stable on any grid, the choice of the grid spacing can be based on the required accuracy. We investigate the accuracy of a fourth-order, symmetry-preserving discretization for the turbulent flow in a channel. The Reynolds number (based on the channel width and the mean bulk velocity) is equal to 5,600. It is shown that with the fourth-order, symmetry-preserving method a $64 \times 64 \times 32$ grid suffices to perform an accurate simulation.

Keywords: Direct Numerical Simulation, Turbulence, Conservation properties and stability, Channel flow.

1. Introduction

In the first half of the nineteenth century, Claude Navier (1822) and George Stokes (1845) derived the equation that governs turbulent flow. 'Their' equation states that the velocity $\boldsymbol{u}$ and pressure $\boldsymbol{p}$ (in an incompressible fluid) are given

D. Drikakis and B.J. Geurts (eds.), Turbulent Flow Computation, 75–100.

by

$$\partial_t \boldsymbol{u} + (\boldsymbol{u} \cdot \nabla)\, \boldsymbol{u} - \tfrac{1}{\mathrm{Re}} \nabla \cdot \nabla \boldsymbol{u} + \nabla p = \boldsymbol{0}, \qquad \nabla \cdot \boldsymbol{u} = 0, \tag{3.1}$$

where the parameter Re denotes the Reynolds number.

Turbulence is created by the non-linear, convective term in this equation. To illustrate this, we consider a velocity field with a x-component given by

$$u = \mathrm{e}^{\mathrm{i}\omega x},$$

and all other components equal zero, for simplicity. This wave (eddy) transports momentum. Its portion is governed by the x-component of the convective term in the Navier-Stokes equations:

$$u \partial_x u = \mathrm{i}\omega \mathrm{e}^{2\mathrm{i}\omega x}$$

Strikingly, the wave-length of this contribution is half that of the velocity *u*. Via the time-derivative in the Navier-Stokes equations this shorter wave-length becomes part of the velocity itself, and thus a smaller scale of motion is created. This process continues, and smaller and smaller scales of motion originate. The cascade ends when the diffusive forces become sufficiently strong to damp the small scales of motion. In our example, the diffusive term in the Navier-Stokes equations reads

$$\tfrac{1}{\mathrm{Re}} \partial_{xx} u = -\tfrac{1}{\mathrm{Re}} \omega^2 \mathrm{e}^{\mathrm{i}\omega x}.$$

As this contribution grows quadratically in terms of ω, it can overtake the convective term, which depends 'only' linearly on ω. The wave-length at which this happens is the smallest wave-length in the flow. In 1922, the meteorologist Lewis Fry Richardson described this process as follows

> *Big whorls have little whorls,*
> *Which feed on their velocity,*
> *And little whorls have lesser whorls,*
> *And so on to viscosity.*

So far, our arguments are heuristic, and not entirely correct, since we have left the time scales out of consideration. This leads to the wrong suggestion that the smallest length scale behaves like Re^{-1}. In 1941, Kolmogorov has considered both time and length scales. He argued that the diffusive term at a somewhat larger length scale, proportional to $\mathrm{Re}^{-3/4}$, is sufficiently strong to end the cascade to smaller scales.

To capture the essence of turbulence in a direct numerical simulation (DNS), the convective term in the Navier-Stokes equations need be discretized with care. The subtle balance between convective transport and diffusive dissipation may be disturbed if the discretization of the convective derivative is stabilized

by means of numerical (artificial) diffusion. With this in mind, we consider the discretization of the convective term in the Navier-Stokes equations. As convection is described by a first-order differential operator, this leads to the apparently simple question how the discretize a first-order derivative.

In mathematical terms: given three values of a smooth function u, say $u_{i-1} = u(x_{i-1})$, $u_i = u(x_i)$ and $u_{i+1} = u(x_{i+1})$ with $x_{i-1} < x_i < x_{i+1}$, find an approximation of the (spatial) derivative of u at x_i. Almost any textbook on numerical analysis answers this question by combining Taylor-series expansions of u around $x = x_i$ in such a manner that as many as possible low-order terms cancel. After some algebraic work this results into the following approximation

$$\partial_x u(x_i) \approx \frac{\delta x_i^2 u_{i+1} + (\delta x_{i+1}^2 - \delta x_i^2) u_i - \delta x_{i+1}^2 u_{i-1}}{\delta x_{i+1} \delta x_i (\delta x_{i+1} + \delta x_i)}, \tag{3.2}$$

where the local spacing of the mesh is denoted by $\delta x_i = x_i - x_{i-1}$. This expression may also be derived by constructing a parabola through the three given data points and differentiating that parabola at $x = x_i$. Expression (3.2) is motivated by the fact that it minimizes the local truncation error at the grid point x_i. But, is this criterion based on sound physical principles? Recalling that the convective term in the Navier-Stokes equations transports energy without dissipating any, and that this transport ends at the scale where diffusion is powerful enough to counterbalance any further transport to smaller scales, we would like that convection conserves the total energy in the discrete form too. This minicing of crucial properties, however, forms a different criterion for discretizing the differential operators in the Navier-Stokes equations, see [1].

Rather than concentrating on reducing local truncation error, we propose to discretize in such a manner that the symmetry of the underlying differential operators is preserved. That is, the convective operator is replaced by a skew-symmetric difference-operator and the diffusive operator is approximated by a symmetric, positive-definite operator. We will show that such a symmetry-preserving discretization of the Navier-Stokes equations is stable on any grid, and conserves the total mass, momentum and kinetic energy (if the physical dissipation is turned off).

Conservation properties of numerical schemes for the (incompressible) Navier-Stokes equations are currently also pursued at other research institutes, in particular in Stanford [2]-[3], at Cerfacs [4], and at Delft University where a variant of our symmetry-preserving discretization for collocated grids has been developed [5]-[6]. Another approach that considers properties such as symmetry, conservation, stability and the relationships between the gradient, divergence and curl operator can be found in [7].

The next section concerns the incompressible Navier-Stokes equations. In this introductory section, we will sketch the main lines of symmetry-preserving

discretization by means of the following, one-dimensional, linear, convection-diffusion equation

$$\partial_t u + \bar{u}\partial_x u - \tfrac{1}{\mathrm{Re}}\partial_{xx} u = 0, \tag{3.3}$$

where the convective transport velocity $\bar{u}$ is taken constant. The time-evolution of the semi-discrete velocity $u_i(t)$ at the grid point x_i reads

$$\boldsymbol{\Omega}_0 \frac{\mathrm{d}\boldsymbol{u}_h}{\mathrm{d}t} + \boldsymbol{C}_0(\bar{u})\boldsymbol{u}_h + \boldsymbol{D}_0\boldsymbol{u}_h = \boldsymbol{0}, \tag{3.4}$$

where the discrete velocities u_i form the vector $\boldsymbol{u}_h$. The diagonal matrix $\boldsymbol{\Omega}_0$ contains the local spacings of the mesh, that is $(\boldsymbol{\Omega}_0)_{i,i} = (x_{i+1} - x_{i-1})/2$. The coefficient matrix $\boldsymbol{C}_0(\bar{u})$ represents the convective operator. When the discretization of the derivative is taken as in (3.2), $\boldsymbol{C}_0(\bar{u})$ becomes a tri-diagonal matrix with entries

$$\boldsymbol{C}_0(\bar{u})_{i,i-1} = -\frac{\bar{u}\delta x_{i+1}}{2\delta x_i}, \qquad \boldsymbol{C}_0(\bar{u})_{i,i+1} = \frac{\bar{u}\delta x_i}{2\delta x_{i+1}}$$

and

$$\boldsymbol{C}_0(\bar{u})_{i,i} = \frac{\bar{u}\delta x_{i+1}}{2\delta x_i} - \frac{\bar{u}\delta x_i}{2\delta x_{i+1}}. \tag{3.5}$$

In the absence of diffusion, that is for $\boldsymbol{D}_0 = \boldsymbol{0}$, the kinetic energy $||\boldsymbol{u}_h||^2 = \boldsymbol{u}_h^* \boldsymbol{\Omega}_0 \boldsymbol{u}_h$ of any solution $\boldsymbol{u}_h$ of the dynamical system (3.4) evolves in time according to

$$\frac{\mathrm{d}}{\mathrm{d}t}||\boldsymbol{u}_h||^2 = -\boldsymbol{u}_h^* \left(\boldsymbol{C}_0(\bar{u}) + \boldsymbol{C}_0^*(\bar{u})\right) \boldsymbol{u}_h.$$

The right hand-side of this expression equals zero for all discrete velocities $\boldsymbol{u}_h$, *i.e.* the energy is conserved unconditionally, if and only if the coefficient matrix $\boldsymbol{C}_0(\bar{u})$ is skew-symmetric:

$$\boldsymbol{C}_0(\bar{u}) + \boldsymbol{C}_0^*(\bar{u}) = \boldsymbol{0}, \tag{3.6}$$

To avoid possible confusion, it may be noted that we use the adjective 'skew-symmetric' to describe a property of the coefficient matrix $\boldsymbol{C}_0(\bar{u})$ of the discrete convective operator. In the literature, the adjective 'skew-symmetric' is also related to a differential formulation of the convective term in the Navier-Stokes equations. The convective term may be written in four different ways (provided that the continuity equation is satisfied). These differential forms are referred to as divergence, advective, skew-symmetric and rotational form. We do not use the adjective 'skew-symmetric' in this context. Note that in our linear example, with a constant convective transport velocity, all differential forms coincide.

To conserve the energy during the convective cascade the coefficient matrix $\boldsymbol{C}_0(\bar{u})$ of the discrete, convective operator has to be a skew-symmetric matrix.

We see immediately that the traditional discretization scheme (3.2) leads to a coefficient matrix that is not skew-symmetric on a non-uniform grid. Indeed, the diagonal entry given by (3.5) is non-zero (unless the grid is uniform). Thus, if the discretization scheme is constructed to minimize the local truncation error, the skew-symmetry of the convective term is lost on non-uniform grids, and quantities that are conserved in the continuous formulation, like the kinetic energy, are not conserved in the discrete formulation.

In general, the symmetric part of $\boldsymbol{C}_0(\bar{u})$ will have both positive and negative eigenvalues. If the discrete velocity $\boldsymbol{u}_h$ is given by a linear combination of eigenvectors corresponding to negative eigenvalues of $\boldsymbol{C}_0(\bar{u}) + \boldsymbol{C}_0^*(\bar{u})$, the kinetic energy increases exponentially in time. Thus, an unconditionally stable solution of the discrete set of equations can not be obtained, unless a damping mechanism is added. Such a mechanism may interfere with the subtle balance between the production of turbulence and its dissipation at the smallest length scales. For that reason, we consider a symmetry-preserving discretization.

To obtain a skew-symmetric, discrete representation of the convective operator, we approximate the convective derivative by

$$\bar{u}\,\partial_x u(x_i) \approx \bar{u}\,\frac{u_{i+1} - u_{i-1}}{x_{i+1} - x_{i-1}} = \left(\boldsymbol{\Omega}_0^{-1}\boldsymbol{C}_0(\bar{u})\boldsymbol{u}_h\right)_i . \tag{3.7}$$

The resulting coefficient matrix $\boldsymbol{C}_0(\bar{u})$ is skew-symmetric on any grid:

$$\boldsymbol{C}_0(\bar{u})_{i,i-1} = -\frac{1}{2}\bar{u}, \qquad \boldsymbol{C}_0(\bar{u})_{i,i} = 0, \qquad \boldsymbol{C}_0(\bar{u})_{i,i+1} = \frac{1}{2}\bar{u}. \tag{3.8}$$

The two ways of discretization, given by (3.2) and (3.7), are illustrated in Figure 3.1. In the symmetry-preserving discretization (3.7) the derivative

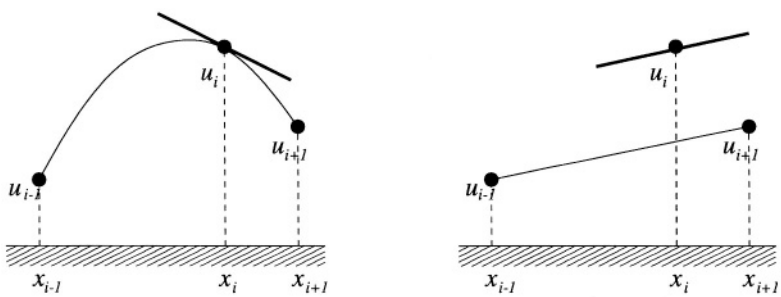

Figure 3.1. Two ways of approximating $\partial_x u$. In the left-hand figure the derivative is approximated by means of a Lagrangian interpolation, that is by Eq. (3.2). In the right-hand figure the symmetry-preserving discretization (3.7) is applied.

$\partial_x u(x_i)$ is simply approximated by drawing a straight line from (x_{i-1}, u_{i-1})

to (x_{i+1}, u_{i+1}). This gives the proper symmetry, but one may get the feeling that this approach is not very accurate. The local truncation error in the approximation of the derivative in (3.7), that is

$$\tau_h(x_i) = \frac{1}{2}(\delta x_{i+1} - \delta x_i)\partial_{xx}u(x_i), + \mathcal{O}(\delta x_{\max}^2) \tag{3.9}$$

is only first-order (unless the grid is almost uniform). Given stability, a sufficient condition for second-order accuracy of the discrete solution u_i is that the local truncation error be second order. Yet, this is not a necessary condition, as is emphasized by Manteufel and White [8]. They have proven that the approximation (3.7) yields second-order accurate solutions on uniform as well as on non-uniform meshes, even though its local truncation error τ_h is formally only first-order on non-uniform meshes. The standard proof (which uses stability and consistency to imply convergence) is inadequate to handle non-uniform meshes. Instead, Manteufel and White [8] argue that the error ϵ_i in the approximation of $u(x_i)$ in (3.7) satisfies $\boldsymbol{C}_0(\bar{u})\boldsymbol{\epsilon}_h = \boldsymbol{\Omega}_0\boldsymbol{\tau}_h$, or written out per element

$$\tfrac{\bar{u}}{2}\epsilon_{i+1} - \tfrac{\bar{u}}{2}\epsilon_{i-1} \overset{(3.7)+(3.9)}{=} \frac{1}{2}(\delta x_{i+1}^2 - \delta x_i^2)\partial_{xx}u(x_i) + (\delta x_{i+1} + \delta x_i)\,\mathcal{O}(\delta x_{\max}^2).$$

The left hand-side of this expression may be written as $\epsilon_{i+1/2} - \epsilon_{i-1/2}$, where $\epsilon_{i+1/2} = (\epsilon_{i+1} + \epsilon_i)\bar{u}/2$. Recurring this error-equation back to an error at a boundary, say $\epsilon_{1/2}$, we have

$$\begin{aligned}
\epsilon_{i+1/2} - \epsilon_{1/2} &= \frac{1}{2}\sum_{k=1}^{i}\left(\delta x_{k+1}^2 - \delta x_k^2\right)\partial_{xx}u(x_k) + \mathcal{O}(\delta x_{\max}^2) \\
&= \frac{1}{2}\sum_{k=1}^{i-1}\delta x_k^2\left(\partial_{xx}u(x_{k-1}) - \partial_{xx}u(x_k)\right) + \mathcal{O}(\delta x_{\max}^2).
\end{aligned}$$

The final sum is itself $\mathcal{O}(\delta x_{\max}^2)$. Thus, the error $\epsilon_{i+1/2}$ is second-order in spite of the first-order truncation error. This implies that ϵ_i itself is second-order.

Here, it may be noted that the skew-symmetric coefficient matrix $\boldsymbol{C}_0(\bar{u})$ in (3.7) may also be derived from a Galerkin finite element method. In that approach the velocity is written as

$$u(x,t) = \sum_i u_i(t)\psi_i(x)$$

where the basis functions $\psi_i(x)$ are piecewise linear functions with $\psi_i(x_i) = 1$ and $\psi_i(x_j) = 0$ for $i \neq j$. For the linear problem (3.3), the coefficients

$$\boldsymbol{C}_0(\bar{u})_{i,j} = \bar{u}\int_0^1 \psi_i(x)\partial_x\psi_j(x)dx$$

are identical to those given by (3.8), and satisfy the symmetry property (3.6) by construction. The difference with the 'finite volume/difference' method (3.4) is that the mass matrix $\tilde{\boldsymbol{\Omega}}_0 = \int_0^1 \psi_i(x)\psi_j(x)dx$ of the finite element method is not a diagonal, but a tri-diagonal matrix. Both methods are identical, when the off-diagonal entries of $\tilde{\boldsymbol{\Omega}}_0$ are lumped to the diagonal.

To construct the coefficient matrix $\boldsymbol{D}_0$ of the diffusive term in (3.4), we rewrite the second-order differential equation (3.4) as a system of two first-order differential equations

$$\partial_t u + \bar{u}\partial_x u - \tfrac{1}{\mathrm{Re}}\partial_x \phi = 0 \qquad \phi = \partial_x u. \tag{3.10}$$

The diffusive flux ϕ is discretized in a standard way:

$$\phi_{i+1/2} = \left(\boldsymbol{\Lambda}_0^{-1}\boldsymbol{\Delta}_0 \boldsymbol{u}_h\right)_i,$$

where the difference matrix $\boldsymbol{\Delta}_0$ is defined by $(\boldsymbol{\Delta}_0\boldsymbol{u}_h)_i = u_i - u_{i-1}$, and the non-zero entries of the diagonal matrix $\boldsymbol{\Lambda}_0$ read $(\boldsymbol{\Lambda}_0)_{i,i} = x_i - x_{i-1}$. The derivative of ϕ is approximated according to

$$\partial_x \phi(x_i) \approx \left(\boldsymbol{\Omega}_0^{-1}\boldsymbol{\Delta}_0^* \boldsymbol{\phi}_h\right)_i,$$

where the vector $\boldsymbol{\phi}_h$ consists of the discrete values of ϕ at the mid-points $x_{i-1/2}$. Eliminating these auxiliary unknowns from the expressions above gives

$$\boldsymbol{D}_0 = \tfrac{1}{\mathrm{Re}}\,\boldsymbol{\Delta}_0^*\,\boldsymbol{\Lambda}_0^{-1}\boldsymbol{\Delta}_0. \tag{3.11}$$

The quadratic form $\boldsymbol{u}_h^* \boldsymbol{D}_0 \boldsymbol{u}_h = \frac{1}{\mathrm{Re}}\,(\boldsymbol{\Delta}_0\boldsymbol{u}_h)^*\,\boldsymbol{\Lambda}_0^{-1}\,(\boldsymbol{\Delta}_0\boldsymbol{u}_h)$ is strictly positive for all $\boldsymbol{\Delta}_0\boldsymbol{u}_h \neq \boldsymbol{0}$ *(i.e.* for all $\boldsymbol{u}_h \neq \alpha\boldsymbol{1}$, where α is an arbitrary constant), since the entries of $\boldsymbol{\Lambda}_0$ are positive. The quadratic form $\boldsymbol{u}_h^*\boldsymbol{D}_0\boldsymbol{u}_h$ is equal to zero if $\boldsymbol{u}_h = \alpha\boldsymbol{1}$. Thus, the matrix $\boldsymbol{D}_0$ is positive-definite, like the underlying differential operator $-\partial_{xx}$.

The symmetric part of $\boldsymbol{C}_0(\bar{u}) + \boldsymbol{D}_0$ is only determined by diffusion, and hence is positive-definite. Under this condition, the evolution of the kinetic energy $||\boldsymbol{u}_h||_h^2 = \boldsymbol{u}_h^*\boldsymbol{\Omega}_0\boldsymbol{u}_h$ of any discrete solution $\boldsymbol{u}_h$ of (3.4) is governed by

$$\begin{aligned}\frac{\mathrm{d}}{\mathrm{dt}}(\boldsymbol{u}_h^*\boldsymbol{\Omega}_0\boldsymbol{u}_h) &\overset{(3.4)}{=} -\boldsymbol{u}_h^*(\boldsymbol{C}_0(\bar{u}) + \boldsymbol{C}_0^*(\bar{u}))\boldsymbol{u}_h - \boldsymbol{u}_h^*(\boldsymbol{D}_0 + \boldsymbol{D}_0^*)\boldsymbol{u}_h \\ &\overset{(3.6)}{=} -\boldsymbol{u}_h^*(\boldsymbol{D}_0 + \boldsymbol{D}_0^*)\boldsymbol{u}_h \leq 0,\end{aligned}$$

where the right-hand side is zero if and only if $\boldsymbol{u}_h$ lies in the null space of $\boldsymbol{D}_0 + \boldsymbol{D}_0^*$. Consequently, a stable solution can be obtained on any grid.

As the eigenvalues of $\boldsymbol{C}_0(\bar{u}) + \boldsymbol{D}_0$ lie in the stable half-plane, this matrix is regular, which is important for the relationship between the global and local

truncation error. To illustrate this, we consider the stationary equivalent of Eq. (3.3): $\bar{u}\partial_x u - \frac{1}{\mathrm{Re}}\partial_{xx} u = 0$. As before, this equation is approximated by $(\boldsymbol{C}_0(\bar{u}) + \boldsymbol{D}_0)\,\boldsymbol{u}_h = \boldsymbol{0}$. To define the global truncation error, we restrict the exact solution to the grid points, first. The vector of these values is denoted by $\boldsymbol{u}$. The global truncation error, defined as $\boldsymbol{u} - \boldsymbol{u}_h$, is equal to the product of the inverse of the discrete operator $\boldsymbol{C}_0(\bar{u}) + \boldsymbol{D}_0$ and the local truncation error. Therefore, a (nearly) singular discrete operator can destroy favourable properties of the local truncation error. Examples of this (for non-symmetry-preserving discretizations!) can be found in [9].

2. Symmetry-preserving discretization

In the preceding section, we saw that the conservation properties and the stability of the spatial discretization of a simple, one-dimensional, convection-diffusion equation (3.3) may be improved when less emphasis is laid upon the local truncation error, so that the symmetry of the underlying differential operators can be respected. In this section, we will extend the symmetry-preserving discretization to the incompressible, Navier-Stokes equations (in two spatial directions only, as the extension to 3D is straightforward).

On a uniform grid the traditional aim, minimize the local truncation error, need not break the symmetry. The well-known, second-order scheme of Harlow and Welsh [10] forms an example of this. In Section 2.1, we will generalize Harlow and Welsh's scheme to non-uniform meshes in such a manner that the symmetries of the convective and diffusive operator are not broken. The conservation properties and stability of the resulting, second-order scheme are discussed in Section 2.2. After that (Section 2.3), we will improve the order of the basic scheme by means of a Richardson extrapolation, just like in [11]. This results into a fourth-order, symmetry-preserving discretization. The last section (Sec. 2.4) concerns the treatment of the boundary conditions.

2.1 Basic, second-order method

In this section we will apply symmetry-preserving discretization to the incompressible Navier-Stokes equations (3.1) in two spatial dimensions. For that, we will use a staggered grid and adopt the notations of Harlow & Welsh [10]. Figure 3.2 illustrates the definition of the discrete velocities $(u_{i,j}, v_{i,j})$.

For an incompressible fluid the mass of any control volume $\Omega_{i,j} = [x_{i-1}, x_i] \times [y_{j-1}, y_j]$ is conserved:

$$\bar{u}_{i,j} + \bar{v}_{i,j} - \bar{u}_{i-1,j} - \bar{v}_{i,j-1} = 0, \tag{3.12}$$

where $\bar{u}_{i,j}$ denotes the mass flux through the face $y = y_j$ of the grid cell $\Omega_{i,j}$ and $\bar{v}_{i,j}$ stands for the mass flux through the grid face $x = x_i$:

$$\bar{u}_{i,j} = \int_{y_{j-1}}^{y_j} u(x_i, y, t)dy \quad \text{and} \quad \bar{v}_{i,j} = \int_{x_{i-1}}^{x_i} v(x, y_j, t)dx. \tag{3.13}$$

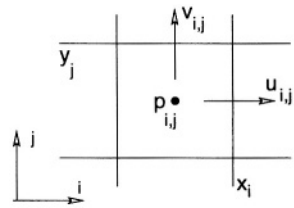

Figure 3.2. The location of the discrete velocities.

The combination (3.12)+(3.13) does not contain a discretization error, since the integrals in (3.13) have not yet been discretized. We postpone their discretization till later in this section. Till then we view the velocities $(u_{i,j}, v_{i,j})$ as the unknowns and the mass fluxes $(\bar{u}_{i,j}, \bar{v}_{i,j})$ as being given such that (3.12) holds.

As mass and momentum are transported at equal velocity, the mass flux is used to discretize the transport velocity of momentum. The (spatial) discretization of the transport of momentum of a region $\Omega_{i+1/2,j} = [x_{i-1/2}, x_{i+1/2}] \times [y_{j-1}, y_j]$ becomes

$$\begin{aligned} |\Omega_{i+1/2,j}|\frac{\mathrm{d}u_{i,j}}{\mathrm{d}t} &+ \bar{u}_{i+1/2,j}u_{i+1/2,j} + \bar{v}_{i+1/2,j}u_{i,j+1/2} \\ &- \bar{u}_{i-1/2,j}u_{i-1/2,j} - \bar{v}_{i+1/2,j-1}u_{i,j-1/2}. \end{aligned} \tag{3.14}$$

The non-integer indices in (3.14) refer to the faces of $\Omega_{i+1/2,j}$. For example, $u_{i-1/2,j}$ stands for the u-velocity at the interface of $\Omega_{i-1/2,j}$ and $\Omega_{i+1/2,j}$. The velocity at a control face is approximated by the average of the velocity at both sides of it:

$$u_{i+1/2,j} = \frac{1}{2}(u_{i+1,j} + u_{i,j}) \quad \text{and} \quad u_{i,j+1/2} = \frac{1}{2}(u_{i,j+1} + u_{i,j}). \tag{3.15}$$

In addition to the set of equations for the u-component of the velocity (3.14)-(3.15), there is an analogous set for the v-component:

$$\begin{aligned} |\Omega_{i,j+1/2}|\frac{\mathrm{d}v_{i,j}}{\mathrm{d}t} &+ \bar{v}_{i,j+1/2}v_{i,j+1/2} + \bar{u}_{i,j+1/2}v_{i+1/2,j} \\ &- \bar{v}_{i,j-1/2}v_{i,j-1/2} - \bar{u}_{i-1,j+1/2}v_{i-1/2,j}, \end{aligned} \tag{3.16}$$

with

$$v_{i+1/2,j} = \frac{1}{2}(v_{i+1,j} + v_{i,j}) \quad \text{and} \quad v_{i,j+1/2} = \frac{1}{2}(v_{i,j+1} + v_{i,j}). \tag{3.17}$$

We conceive Eqs. (3.14)-(3.17) as expressions for the velocities, where the mass fluxes $\bar{u}$ and $\bar{v}$ form the coefficients. Thus, we can write the (semi-

)discretization in matrix-vector notation as

$$\boldsymbol{\Omega}_1 \frac{\mathrm{d}\boldsymbol{u}_h}{\mathrm{d}t} + \boldsymbol{C}_1(\bar{\boldsymbol{u}})\boldsymbol{u}_h,$$

where $\boldsymbol{u}_h$ denotes the discrete velocity-vector (which consists of both the $u_{i,j}$'s and $v_{i,j}$'s), $\boldsymbol{\Omega}_1$ is a (positive-definite) diagonal matrix representing the sizes of the control volumes $|\Omega_{i+1/2,j}|$ and $|\Omega_{i,j+1/2}|$, whereas $\boldsymbol{C}_1(\bar{\boldsymbol{u}})$ is built from the flux contributions through the control faces, *i.e.* $\boldsymbol{C}_1$ depends on the mass fluxes $\bar{u}$ and $\bar{v}$ at the control faces.

With no (in- or external) force, the discrete transport equation

$$\boldsymbol{\Omega}_1 \frac{\mathrm{d}\boldsymbol{u}_h}{\mathrm{d}t} + \boldsymbol{C}_1(\bar{\boldsymbol{u}})\boldsymbol{u}_h = \boldsymbol{0} \tag{3.18}$$

conserves the discrete energy $\boldsymbol{u}_h^* \boldsymbol{\Omega}_1 \boldsymbol{u}_h$ (of any discrete velocity field u_h), that is

$$\frac{\mathrm{d}}{\mathrm{d}t}\left(\boldsymbol{u}_h^* \boldsymbol{\Omega}_1 \boldsymbol{u}_h\right) \overset{(3.18)}{=} -\boldsymbol{u}_h^* \left(\boldsymbol{C}_1(\bar{\boldsymbol{u}}) + \boldsymbol{C}_1^*(\bar{\boldsymbol{u}})\right) \boldsymbol{u}_h = 0, \tag{3.19}$$

if and only if the coefficient matrix $\boldsymbol{C}_1(\bar{\boldsymbol{u}})$ is skew-symmetric:

$$\boldsymbol{C}_1(\bar{\boldsymbol{u}}) + \boldsymbol{C}_1^*(\bar{\boldsymbol{u}}) = \boldsymbol{0}. \tag{3.20}$$

This condition is verified in two steps. To start, we consider the off-diagonal elements. The matrix $\boldsymbol{C}_1(\bar{\boldsymbol{u}}) - \mathrm{diag}(\boldsymbol{C}_1(\bar{\boldsymbol{u}}))$ is skew-symmetric if and only if the weights in the interpolations (3.15) and (3.17) of the discrete velocities are taken constant. On a non-uniform grid one would be tempted to tune the weights $\frac{1}{2}$ in Eqs. (3.15) and (3.17) to the local mesh sizes to minimize the local truncation error. Yet, this breaks the skew-symmetry. Indeed, suppose we would follow the Lagrangian approach by taking

$$u_{i+1/2,j} = (1 - \omega_{i,j})u_{i+1,j} + \omega_{i,j}u_{i,j}$$

instead of (3.15), where the coefficient $\omega_{i,j}$ depends on the local mesh sizes. Then, by substituting this mesh-dependent interpolation rule into Eq. (3.14) we see that the coefficient of $u_{i+1,j}$ becomes $(1 - \omega_{i,j})\bar{u}_{i+1/2,j}$, while the term $u_{i-1/2,j}\bar{u}_{i-1/2,j}$ in (3.14) with i replaced by $i + 1$ yields the coefficient $-\omega_{i,j}\bar{u}_{i+1/2,j}$ for $u_{i,j}$. For skew-symmetry, these two coefficients should be of opposite sign. That is, we should have

$$(1 - \omega_{i,j})\bar{u}_{i+1/2,j} = \omega_{i,j}\bar{u}_{i+1/2,j},$$

for all mass fluxes $\bar{u}_{i+1/2,j}$. This can only be achieved when the weight $\omega_{i,j}$ is taken equal to the uniform weight $\omega_{i,j} = 1/2$, hence independent of the grid location. Therefore we take constant weights in Eqs. (3.15) and (3.17),

also on non-uniform grids. Here, it may be noted that it is either one or the other: either the discretization is selected on basis of its formal, local truncation error (that is, the interpolation is adapted to the local grid spacings) or the skew-symmetry is preserved. For skew-symmetry, the convective flux through the common interface between two neighbouring control volumes has to be computed independent of the control volume in which it is considered.

Next, we consider the diagonal of $\boldsymbol{C}_1$. In the notation above, we have suppressed the argument $\bar{\boldsymbol{u}}$ of $\boldsymbol{C}_1$, because $\boldsymbol{C}_1 - \mathrm{diag}(\boldsymbol{C}_1)$ is skew-symmetric for all $\bar{\boldsymbol{u}}$. The interpolation rule for the mass fluxes $\bar{u}$ and $\bar{v}$ through the faces of the control volumes is determined by the requirement that the diagonal of $\boldsymbol{C}_1$ has to be zero. Then, we have (3.20). By substituting (3.15) into (3.14) we obtain the diagonal element

$$\frac{1}{2}\left(\bar{u}_{i+1/2,j} + \bar{v}_{i+1/2,j} - \bar{u}_{i-1/2,j} - \bar{v}_{i+1/2,j-1}\right). \tag{3.21}$$

This expression is equal to a linear combination of left-hand sides of Eq. (3.12) if the mass fluxes in (3.14) are interpolated to the faces of a u-cell according to

$$\bar{u}_{i+1/2,j} = \frac{1}{2}(\bar{u}_{i+1,j} + \bar{u}_{i,j}) \quad \text{and} \quad \bar{v}_{i+1/2,j} = \frac{1}{2}(\bar{v}_{i+1,j} + \bar{v}_{i,j}). \tag{3.22}$$

It goes without saying that this interpolation rule is also applied in the j-direction to approximate the mass flux through the faces of v-cells. Thus, the coefficient matrix $\boldsymbol{C}_1$ is skew-symmetric if Eq. (3.12) holds, and if the discrete velocities $\boldsymbol{u}_h$ and fluxes $\bar{\boldsymbol{u}}$ are interpolated to the surfaces of control cells with weights $\frac{1}{2}$, as in Eqs. (3.15) and (3.22).

The matrix $\boldsymbol{C}_1(\bar{\boldsymbol{u}})$ is skew-symmetric for any relation between $\bar{\boldsymbol{u}}$ and $\boldsymbol{u}_h$. Obviously, the mass flux $\bar{\boldsymbol{u}}$ has to be expressed in terms of the discrete velocity vector $\boldsymbol{u}_h$ in order to close the system of equations (3.18). The coefficient matrix $\boldsymbol{C}_1(\bar{\boldsymbol{u}})$ becomes a function of the discrete velocity $\boldsymbol{u}_h$ then. We will make liberal use of its name, and denote the resulting coefficient matrix by $\boldsymbol{C}_1(\boldsymbol{u}_h)$. The mass fluxes $\bar{u}_{i,j}$ and $\bar{v}_{i,j}$ are approximated by means of the mid-point rule:

$$\bar{u}_{i,j} = (y_j - y_{j-1})u_{i,j} \quad \text{and} \quad \bar{v}_{i,j} = (x_i - x_{i-1})v_{i,j}. \tag{3.23}$$

The continuity equation (3.12) may then be written in terms of the discrete velocity vector $\boldsymbol{u}_h$. We will denote the coefficient matrix by $\boldsymbol{M}_1$. Hence, the discretization of the continuity equation reads $\boldsymbol{M}_1\boldsymbol{u}_h$ = given, where the right-hand side depends upon the boundary conditions. It is formed by those parts of (3.12) that correspond to mass fluxes through the boundary of the computational domain. To keep the expressions simple, we take the right-hand side equal to zero, *i.e.* we consider no-slip or periodical boundary conditions. Other boundary conditions can be treated likewise (at the expense of some additional terms in the expressions to follow).

The surface integrals that result after that the pressure gradient in the Navier-Stokes equations is integrated over the control volumes for the discrete velocities are discretized by the same rule that is applied to discretize the mass fluxes $\bar{u}_{i,j}$ and $\bar{v}_{i,j}$. Then, the coefficient matrix of the discrete pressure gradient becomes $-(\boldsymbol{\Omega}_1)^{-1}\boldsymbol{M}_1^*$. That is, apart from a diagonal scaling (by $-(\boldsymbol{\Omega}_1)^{-1}$), the coefficient matrix of the discrete gradient operator is given by the transpose of the discrete divergence.

In the continuous case diffusion corresponds to a symmetric, positive-definite operator. In our approach we want this property to hold also for the discrete diffusive operator. To that end, we view the underlying, second-order differential operator as the product of two first-order differential operators, a divergence and a gradient. We discretize the divergence operator. The discrete gradient is constructed from that by taking the transpose of the discrete divergence and multiplying that by a diagonal scaling. This leads to a symmetric, positive-definite, approximation of the diffusive fluxes. We will work this out for the diffusive flux through the faces of the control volume $\Omega_{i+1/2,j}$ for the discrete velocity $u_{i,j}$. To start, we introduce the fluxes

$$\bar{\phi}_{i+1/2,j} = \int_{y_{j-1}}^{y_j} \phi\left(x_{i+1/2}, y\right) dy \quad \text{and} \quad \bar{\psi}_{i,j} = \int_{x_{i-1/2}}^{x_{i+1/2}} \psi\left(x, y_j\right) dx,$$

where $\phi = \partial_x u$ and $\psi = \partial_y u$. In terms of these surface integrals the diffusive flux through the faces of the control volume $\Omega_{i+1/2,j}$ of $u_{i,j}$ reads

$$\tfrac{1}{\mathrm{Re}}\left(\bar{\phi}_{i+1/2,j} - \bar{\phi}_{i-1/2,j} + \bar{\psi}_{i,j} - \bar{\psi}_{i,j-1}\right).$$

The surface integrals in this expression are approximated according to

$$\bar{\phi}_{i+1/2,j} = (y_j - y_{j-1})\phi_{i+1/2,j} \quad \text{and} \quad \bar{\psi}_{i,j} = (x_{i+1/2} - x_{i-1/2})\psi_{i,j}.$$

In matrix-vector notation, the diffusive flux through the faces of u-cells is given by $\boldsymbol{M}_1^u\boldsymbol{\phi}_h$, where the vector $\boldsymbol{\phi}_h$ consists of the $\phi_{i+1/2,j}$'s and $\psi_{i,j}$'s. The coefficient matrix $\boldsymbol{M}_1^u$ may be constructed out of $\boldsymbol{M}_1$, by lowering $\boldsymbol{M}_1$'s dimension in the x-direction by one, and replacing $x_i - x_{i-1}$ by $x_{i+1/2} - x_{i-1/2}$. The difference between $\boldsymbol{M}_1^u$ and $\boldsymbol{M}_1$ is due to the staggering of the grid: the discrete divergence operator $\boldsymbol{M}_1^u$ works on the control cells $\Omega_{i+1/2,j}$ for u-momentum, whereas $\boldsymbol{M}_1$ operates on the grid cells $\Omega_{i,j}$. The gradient operator relating ϕ and ψ to the velocity component u is discretized by $-(\boldsymbol{\Omega}_1^u)^{-1}(\boldsymbol{M}_1^u)^*$, where the entries of the diagonal matrix $\boldsymbol{\Omega}_1^u$ are given by $|\Omega_{i,j}|$ and $|\Omega_{i,j+1/2}|$. We need to introduce this diagonal matrix, because the staggering of the grid yields different control volumes for the transport of mass and momentum: $\boldsymbol{\Omega}_1^u$ may be constructed out of $\boldsymbol{\Omega}_1$ by replacing the entries $|\Omega_{i+1/2,j}|$ with $|\Omega_{i,j}|$. The diffusive flux through v-cells is approximated similarly. It's coefficient

matrix reads $\frac{1}{\mathrm{Re}} \boldsymbol{M}_1^v \left(\boldsymbol{\Omega}_1^v\right)^{-1} \left(\boldsymbol{M}_1^v\right)^*$, where $\boldsymbol{M}_1^v$ may be obtained from M_1 by lowering $\boldsymbol{M}_1$'s y-dimension by one, and replacing $y_j - y_{j-1}$ by $y_{j+1/2} - y_{j-1/2}$; The diagonal matrix $\boldsymbol{\Omega}_1^v$ represents the sizes $|\Omega_{i+1/2,j}|$ and $|\Omega_{i,j}|$. So, the symmetric, positive-definite differential operator $-\frac{1}{\mathrm{Re}} \nabla \bullet \nabla u$ in the Navier-Stokes equations (3.1) is discretized by $\boldsymbol{\Omega}_1^{-1} \boldsymbol{D}_1 \boldsymbol{u}_h$, where the coefficient matrix $\boldsymbol{D}_1$ is given by

$$\boldsymbol{D}_1 = \tfrac{1}{\mathrm{Re}} \boldsymbol{\Delta}_1^* \boldsymbol{\Lambda}_1^{-1} \boldsymbol{\Delta}_1 \quad \text{with} \quad \boldsymbol{\Delta}_1^* = \begin{pmatrix} \boldsymbol{M}_1^u & \boldsymbol{0} \\ \boldsymbol{0} & \boldsymbol{M}_1^v \end{pmatrix} \tag{3.24}$$

and $\boldsymbol{\Lambda}_1 = \mathrm{diag}\left(\boldsymbol{\Omega}_1^u, \boldsymbol{\Omega}_1^v\right)$. The matrix $\boldsymbol{D}_1$ is symmetric, (weakly) diagonal dominant, has positive entries at its diagonal, and negative off-diagonal elements. Hence, $\boldsymbol{D}_1$ is an M-matrix.

By adding viscous and pressure forces to the discrete transport equation (3.18), we obtain the following semi-discrete representation of the incompressible Navier-Stokes equations

$$\boldsymbol{\Omega}_1 \frac{\mathrm{d}\boldsymbol{u}_h}{\mathrm{d}t} + \boldsymbol{C}_1(\boldsymbol{u}_h)\boldsymbol{u}_h + \boldsymbol{D}_1 \boldsymbol{u}_h - \boldsymbol{M}_1^* \boldsymbol{p}_h = \boldsymbol{0}, \qquad \boldsymbol{M}_1 \boldsymbol{u}_h = 0, \tag{3.25}$$

where the vector $\boldsymbol{p}_h$ represents the discrete pressure.

2.2 Conservation properties and stability

The total mass and momentum of a flow are conserved analytically. Without diffusion, the kinetic energy is conserved too. With diffusion, the kinetic energy decreases in time. The coefficient matrices in the semi-discretization (3.25) are constructed such that these conservation and stability properties hold also for the discrete solution, as will be shown in this section.

The total mass of the semi-discrete flow is trivially conserved. Its total amount of momentum evolves in time according to

$$\frac{\mathrm{d}}{\mathrm{d}t}\left(\boldsymbol{1}^* \boldsymbol{\Omega}_1 \boldsymbol{u}_h\right) \overset{(3.25)}{=} -\boldsymbol{1}^* \left(\boldsymbol{C}_1(\boldsymbol{u}_h) + \boldsymbol{D}_1\right) \boldsymbol{u}_h + \boldsymbol{1}^* \boldsymbol{M}_1^* \boldsymbol{p}_h,$$

where the vector 1 has as many entries as there are control volumes for the discrete velocity components $u_{i,j}$ and $v_{i,j}$. Hence, momentum is conserved for any discrete velocity $\boldsymbol{u}_h$ and discrete pressure $\boldsymbol{p}_h$, if the coefficient matrices $\boldsymbol{C}_1(\boldsymbol{u}_h)$, $\boldsymbol{D}_1$ and $\boldsymbol{M}_1$ satisfy

$$\boldsymbol{C}_1^*(\boldsymbol{u}_h)\boldsymbol{1} = \boldsymbol{0} \qquad \boldsymbol{D}_1^* \boldsymbol{1} = \boldsymbol{0} \qquad \text{and} \qquad \boldsymbol{M}_1 \boldsymbol{1} = \boldsymbol{0}. \tag{3.26}$$

The latter of these three conditions expresses that a constant (discrete) velocity field has to satisfy the law of conservation of mass. Obviously, this condition

is satisfied. The first two conditions in Eq. (3.26) can be viewed as consistency conditions too. Indeed, we may leave the transposition in these conditions away, since $\boldsymbol{C}_1(\boldsymbol{u}_h)$ is skew-symmetric and $\boldsymbol{D}_1$ is symmetric. So it suffices to verify that the row-sums of $\boldsymbol{C}_1(\boldsymbol{u}_h)$ and $\boldsymbol{D}_1$ are zero. Those of $\boldsymbol{D}_1$ are zero by definition. The row-sums of $\boldsymbol{C}_1(\boldsymbol{u}_h)$ can be worked out from (3.14)+(3.15). Each row-sum is equal to two times the corresponding diagonal element, and thus zero, since $\boldsymbol{C}_1(\boldsymbol{u}_h)$ is skew-symmetric.

Without diffusion ($\boldsymbol{D}_1 = \boldsymbol{0}$), the kinetic energy $\boldsymbol{u}_h^* \boldsymbol{\Omega}_1 \boldsymbol{u}_h$ of any solution of (3.25) is conserved as the coefficient matrix $\boldsymbol{C}_1(\boldsymbol{u}_h)$ is skew-symmetric:

$$\begin{aligned} \frac{\mathrm{d}}{\mathrm{d}t}\left(\boldsymbol{u}_h^* \boldsymbol{\Omega}_1 \boldsymbol{u}_h\right) &\overset{(3.25)}{=} -\boldsymbol{u}_h^* \left(\boldsymbol{C}_1(\boldsymbol{u}_h) + \boldsymbol{C}_1^*(\boldsymbol{u}_h)\right) \boldsymbol{u}_h \\ &+ \left(\boldsymbol{M}_1 \boldsymbol{u}_h\right)^* \boldsymbol{p}_h + \boldsymbol{p}_h^* \left(\boldsymbol{M}_1 \boldsymbol{u}_h\right) = 0. \end{aligned}$$

The two conditions (3.20) and (3.26) imposed on $\boldsymbol{C}_1(\boldsymbol{u}_h)$ reflect that it represents a discrete gradient: its null space consists of the vectors $\alpha \boldsymbol{1}$, with α constant, and $\boldsymbol{C}_1(\boldsymbol{u}_h)$ is skew-symmetric, like a first-order differential operator.

Furthermore, it may be remarked that the pressure does not effect the evolution of the kinetic energy, because the discrete pressure gradient is represented by the transpose of the coefficient matrix $\boldsymbol{M}_1$ of the law of conservation of mass. Formally, the contribution of the pressure to the evolution of the energy reads

$$\boldsymbol{u}_h^* \left(\boldsymbol{M}_1^* \boldsymbol{p}_h\right) + \left(\boldsymbol{M}_1^* \boldsymbol{p}_h\right)^* \boldsymbol{u}_h = \left(\boldsymbol{M}_1 \boldsymbol{u}_h\right)^* \boldsymbol{p}_h + \boldsymbol{p}_h^* \left(\boldsymbol{M}_1 \boldsymbol{u}_h\right).$$

As this expression equals zero (on condition that $\boldsymbol{M}_1 \boldsymbol{u}_h = \boldsymbol{0}$), the pressure can not unstabilize the spatial discretization.

The coefficient matrix $\boldsymbol{D}_1$ of the discrete diffusive operator inherits its symmetry and definiteness from the underlying Laplacian differential operator. Consequently, with diffusion (that is for $\boldsymbol{D}_1 \neq \boldsymbol{0}$) the energy $\boldsymbol{u}_h^* \boldsymbol{\Omega}_1 \boldsymbol{u}_h$ of any solution $\boldsymbol{u}_h$ of the semi-discrete system (3.25) decreases in time unconditionally:

$$\frac{\mathrm{d}}{\mathrm{d}t}(\boldsymbol{u}_h^* \boldsymbol{\Omega}_1 \boldsymbol{u}_h) = -\boldsymbol{u}_h^* (\boldsymbol{D}_1 + \boldsymbol{D}_1^*) \boldsymbol{u}_h < 0,$$

where the right-hand side is negative for all $\boldsymbol{u}_h$'s (except those that lie in the null space of $\boldsymbol{D}_1 + \boldsymbol{D}_1^*$), because the matrix $\boldsymbol{D}_1 + \boldsymbol{D}_1^*$ is positive-definite. This implies that the semi-discrete system (3.25) is stable. Since a solution can be obtained on any grid, we need not add an artificial dissipation mechanism. The grid may be chosen on basis of the required accuracy. But, how accurate is (3.25)? This question will be addressed in Section 3. First, we will further enhance its accuracy.

2.3 Higher-order, symmetry-preserving approximation

To turn Eq. (3.14) into a higher-order approximation, we write down the transport of momentum of a region $\Omega^{(3)}_{i+1/2,j} = [x_{i-3/2}, x_{i+3/2}] \times [y_{j-2}, y_{j+1}]$. Here, it may be noted that we can not blow up the 'original' volumes $\Omega_{i+1/2,j}$ by a factor of two (in all directions) since our grid is not collocated. On a staggered grid, three times larger volumes are the smallest ones possible for which the same discretization rule can be applied as for the 'original' volumes. This yields

$$\begin{aligned} |\Omega^{(3)}_{i+1/2,j}|\frac{\mathrm{d}u_{i,j}}{\mathrm{d}t} \quad &+ \quad \bar{\bar{u}}_{i+3/2,j}u_{i+3/2,j} + \bar{\bar{v}}_{i+1/2,j+1}u_{i,j+3/2} \\ &- \quad \bar{\bar{u}}_{i-3/2,j}u_{i-3/2,j} - \bar{\bar{v}}_{i+1/2,j-2}u_{i,j-3/2}, \end{aligned} \tag{3.27}$$

where

$$\bar{\bar{u}}_{i,j} = \int_{y_{j-2}}^{y_{j+1}} u(x_i, y, t)dy \quad \text{and} \quad \bar{\bar{v}}_{i,j} = \int_{x_{i-2}}^{x_{i+1}} v(x, y_j, t)dy.$$

The velocities at the control faces of the large volumes are interpolated to the control faces in a way similar to that given by (3.15):

$$u_{i+3/2,j} = \frac{1}{2}(u_{i+3,j} + u_{i,j}) \quad \text{and} \quad u_{i,j+3/2} = \frac{1}{2}(u_{i,j+3} + u_{i,j}). \tag{3.28}$$

We conceive Eq. (3.26) as an expression for the velocities, where the mass fluxes $\bar{\bar{u}}$ and $\bar{\bar{v}}$ form the coefficients. Considering it like that, we can recapitulate the equations above (together with the analogous set for the v-component) by

$$\boldsymbol{\Omega}_3\frac{\mathrm{d}\boldsymbol{u}_h}{\mathrm{d}t} + \boldsymbol{C}_3(\bar{\bar{\boldsymbol{u}}})\boldsymbol{u}_h, \tag{3.29}$$

where the diagonal matrix $\boldsymbol{\Omega}_3$ represents the sizes of the large control volumes and $\boldsymbol{C}_3$ consists of flux contributions ($\bar{\bar{u}}$ and $\bar{\bar{v}}$) through the faces of these volumes.

On a uniform grid the local truncation errors in (3.18) and (3.29) are of the order $2 + d$, where $d = 2$ in two spatial dimensions and $d = 3$ in 3D. The leading term in the discretization error may be removed through a Richardson extrapolation (just like in [11]). This leads to the fourth-order approximation

$$\boldsymbol{\Omega}\frac{\mathrm{d}\boldsymbol{u}_h}{\mathrm{d}t} + \left(3^{2+d}\boldsymbol{C}_1(\bar{\boldsymbol{u}}) - \boldsymbol{C}_3(\bar{\bar{\boldsymbol{u}}})\right)\boldsymbol{u}_h,$$

where $\boldsymbol{\Omega} = 3^{2+d}\boldsymbol{\Omega}_1 - \boldsymbol{\Omega}_3$. The coefficient matrix of the convective operator depends on both $\bar{\boldsymbol{u}}$ and $\bar{\bar{\boldsymbol{u}}}$, since it is constructed out of $\boldsymbol{C}_1$ and $\boldsymbol{C}_3$. The diffusive

term of the Navier-Stokes equations undergoes a similar treatment. This leads to a fourth-order coefficient matrix

$$\boldsymbol{D} = \tfrac{1}{\mathrm{Re}} \left(3^{2+d}\boldsymbol{\Delta}_1 - \boldsymbol{\Delta}_3\right)^* \left(3^{2+d}\boldsymbol{\Lambda}_1 - \boldsymbol{\Lambda}_3\right)^{-1} \left(3^{2+d}\boldsymbol{\Delta}_1 - \boldsymbol{\Delta}_3\right)$$

where the difference matrix $\boldsymbol{\Delta}_3$ and the diagonal matrix $\boldsymbol{\Lambda}_3$ are the relatives of $\boldsymbol{\Delta}_1$ and $\boldsymbol{\Lambda}_1$ respectively, with the difference that they are defined on 3^d-times larger control volumes. In terms of the abbreviations $\boldsymbol{\Delta} = 3^{2+d}\boldsymbol{\Delta}_1 - \boldsymbol{\Delta}_3$ and $\boldsymbol{\Lambda} = 3^{2+d}\boldsymbol{\Lambda}_1 - \boldsymbol{\Lambda}_3$ we have $\boldsymbol{D} = \frac{1}{\mathrm{Re}}\boldsymbol{\Delta}^*\boldsymbol{\Lambda}^{-1}\boldsymbol{\Delta}$. The quadratic form

$$\boldsymbol{u}_h^* \boldsymbol{D} \boldsymbol{u}_h = \tfrac{1}{\mathrm{Re}} \left(\boldsymbol{\Delta}\boldsymbol{u}_h\right)^* \boldsymbol{\Lambda}^{-1} \left(\boldsymbol{\Delta}\boldsymbol{u}_h\right)$$

is non-negative provided that the entries of the diagonal matrix $\boldsymbol{\Lambda}$ are non-negative. Here, we assume that the grid is chosen such that this condition is satisfied. Note that $\boldsymbol{\Lambda}_{ii} < 0$ for some i implies that the grid is so irregular that is does not make sense to apply a fourth-order method; in that case the second-order method (3.25) should be applied. For $\boldsymbol{\Lambda} > \boldsymbol{0}$, the quadratic form $\boldsymbol{u}_h^* \boldsymbol{D} \boldsymbol{u}_h$ equals zero if and only if $\boldsymbol{\Delta}\boldsymbol{u}_h = \boldsymbol{0}$, that is if and only if the discrete gradient of the velocity equals zero. This is precisely the condition that need be satisfied in the continuous case. Indeed, there we have

$$-\int \boldsymbol{u} \nabla \cdot \nabla \boldsymbol{u} dV = \int |\nabla \boldsymbol{u}|^2 dV = 0$$

if and only if $\nabla \boldsymbol{u} = \boldsymbol{0}$.

To eliminate the leading term of the discretization error in the continuity equation, we apply the law of conservation of mass to $\Omega_{i,j}^{(3)} = [x_{i-2}, x_{i+1}] \times [y_{j-2}, y_{j+1}]$:

$$\bar{\bar{u}}_{i+1,j} + \bar{\bar{v}}_{i,j+1} - \bar{\bar{u}}_{i-2,j} - \bar{\bar{v}}_{i,j-2} = 0. \tag{3.30}$$

As noted before, the matrix $\boldsymbol{C}_1 - \mathrm{diag}(\boldsymbol{C}_1)$ is skew-symmetric, because the velocities at the control faces are interpolated with constant coefficients. The same holds for $\boldsymbol{C}_3$. The matrix $\boldsymbol{C}_3 - \mathrm{diag}(\boldsymbol{C}_3)$ is skew-symmetric for all interpolations of $\bar{\bar{u}}$ and $\bar{\bar{v}}$ to the control faces, since the velocities at the control faces are interpolated with constant coefficients, see (3.28). Hence, without its diagonal the coefficient matrix $3^{2+d}\boldsymbol{C}_1(\bar{\boldsymbol{u}}) - \boldsymbol{C}_3(\bar{\bar{\boldsymbol{u}}})$ is skew-symmetric. By substituting the interpolation (3.28) into the semi-discretization (3.26), we obtain the diagonal element

$$\begin{aligned} 3^{d+2} \quad & \frac{1}{2}(\bar{u}_{i+1/2,j} + \bar{v}_{i+1/2,j} - \bar{u}_{i-1/2,j} - \bar{v}_{i+1/2,j-1}) \\ - \quad & \frac{1}{2}(\bar{\bar{u}}_{i+3/2,j} + \bar{\bar{v}}_{i+1/2,j+1} - \bar{\bar{u}}_{i-3/2,j} - \bar{\bar{v}}_{i+1/2,j-2}). \end{aligned} \tag{3.31}$$

For skew-symmetry the interpolation of the $\bar{u}$'s, $\bar{v}$'s, $\bar{\bar{u}}$'s and $\bar{\bar{v}}$'s to the control faces has to be performed in such a way that the diagonal entries of $3^{2+d}\boldsymbol{C}_1(\bar{\boldsymbol{u}})-\boldsymbol{C}_3(\bar{\bar{\boldsymbol{u}}})$ become equal to zero, that is equal to linear combinations of (3.12) and (3.30). To achieve this, we interpolate $\bar{u}_{i+1/2,j}$ in the following manner

$$\bar{u}_{i+1/2,j} = \frac{1}{2}\alpha(\bar{u}_{i+1,j} + \bar{u}_{i,j}) + \frac{1}{2}(1-\alpha)(\bar{u}_{i+2,j} + \bar{u}_{i-1,j}) \qquad (3.32)$$

where α is a constant, and interpolate $\bar{v}_{i+1/2,j}$, $\bar{\bar{u}}_{i+1/2,j}$ and $\bar{\bar{v}}_{i+1/2,j}$ likewise. We take $\alpha = 9/8$ because all interpolations are fourth-order accurate then (on a uniform grid). Note that we can not take $\alpha = 1$ here (as in Eq. (3.22)) since a Richardson extrapolation does not eliminate the leading term in the truncation error of $\bar{\bar{u}}_{i+1/2,j}$ and $\bar{\bar{v}}_{i+1/2,j}$. The interpolation rule (3.32) is also applied in the j-direction to approximate the flux through the faces of v-cells.

The fluxes $\bar{\bar{u}}_{i,j}$ and $\bar{\bar{v}}_{i,j}$ are approximated, so that they can be expressed in terms of the discrete velocities $u_{i,j}$ and $v_{i,j}$, respectively:

$$\bar{\bar{u}}_{i,j} = (y_{j+1} - y_{j-2})u_{i,j} \quad \text{and} \quad \bar{\bar{v}}_{i,j} = (x_{i+1} - x_{i-2})v_{i,j}. \qquad (3.33)$$

Hence, on a uniform grid, the fluxes $\bar{\bar{u}}_{i,j}$ and $\bar{\bar{v}}_{i,j}$ are approximated by means of the mid-point rule. In matrix-vector notation, we may summarize the discretization of the law of conservation of mass applied to the volumes $\Omega^{(3)}_{i,j}$ by an expression of the form $\boldsymbol{M}_3\boldsymbol{u}_h = \boldsymbol{0}$. The fourth-order approximation of the law of conservation of mass becomes

$$\boldsymbol{M}\boldsymbol{u}_h = (3^{2+d}\boldsymbol{M}_1 - \boldsymbol{M}_3)\boldsymbol{u}_h = \boldsymbol{0}. \qquad (3.34)$$

The weights 3^{2+d} and -1 are to be used on non-uniform grids too, since otherwise the symmetry of the underlying differential operator is lost.

After that the interpolation rule (3.32) is applied, and the flux is expressed in terms of the discrete velocity like in (3.23) and (3.33), the coefficient matrix $3^{2+d}\boldsymbol{C}_1(\bar{\boldsymbol{u}}) - \boldsymbol{C}_3(\bar{\bar{\boldsymbol{u}}})$ becomes a function of the discrete velocity vector $\boldsymbol{u}_h$ only. We will denote that function by $\boldsymbol{C}(\boldsymbol{u}_h)$. Then, the symmetry-preserving discretization of the Navier-Stokes equations (3.1) reads

$$\boldsymbol{\Omega}\frac{\mathrm{d}\boldsymbol{u}_h}{\mathrm{d}t} + \boldsymbol{C}(\boldsymbol{u}_h)\boldsymbol{u}_h + \boldsymbol{D}\boldsymbol{u}_h - \boldsymbol{M}^*\boldsymbol{p}_h = \boldsymbol{0}, \qquad \boldsymbol{M}\boldsymbol{u}_h = 0, \qquad (3.35)$$

where the coefficient matrices $\boldsymbol{C}(\boldsymbol{u}_h), \boldsymbol{D}$ and $\boldsymbol{M}$ are constructed such that the consistency

$$\boldsymbol{C}^*(\boldsymbol{u}_h)\,\boldsymbol{1} = \boldsymbol{0}, \qquad \boldsymbol{D}^*\boldsymbol{1} = \boldsymbol{0} \quad \text{and} \quad \boldsymbol{M}\boldsymbol{1} = \boldsymbol{0} \qquad (3.36)$$

and symmetry

$$\boldsymbol{C}(\boldsymbol{u}_h) + \boldsymbol{C}^*(\boldsymbol{u}_h) = \boldsymbol{0}, \qquad \boldsymbol{D} + \boldsymbol{D}^* \text{ positive-definite}. \qquad (3.37)$$

conditions are fulfiled. These conditions guarantee that the discretization is fully conservative and stable.

2.4 Boundary conditions

So far, we have left the boundary conditions out of consideration. Their numerical treatment has to maintain the symmetry properties. In case of periodic conditions, the discretization can be extended up to the boundaries in a natural way. This does not break the symmetries of the coefficient matrices $\boldsymbol{C}$ and $\boldsymbol{D}$ nor does it conflict with the consistency conditions given in (3.36). Thus for periodic boundary conditions conservation properties are maintained.

For non-periodic boundary conditions, the requirement $\boldsymbol{M}\mathbf{1} = \mathbf{0}$ can be met by defining the velocities that form part of the stencil (3.30) and fall outside the flow domain in such a way that (3.30) holds for a constant velocity. At a no-slip wall this can be achieved by mirroring both the grid and velocity normal to the wall. For example, at a wall $y = 0$ the missing, out-of-domain velocity is defined by $u(x, -y) = u(x, y)$. Implicitly, this also defines the out-of-domain pressures. Indeed, by defining $\boldsymbol{M}\boldsymbol{u}_h$ near a boundary we define $\boldsymbol{M}^*\boldsymbol{p}_h$ too.

The discretization of the convective fluxes near the boundaries has to be done such that (a) the skew-symmetry of $\boldsymbol{C}$ is preserved and (b) the row-sums of $\boldsymbol{C}$ are zero (provided that $\boldsymbol{M}\boldsymbol{u}_h = \mathbf{0}$). To satisfy these two conditions at a no-slip boundary, we mirror the velocity in the no-slip wall (as before). The mirroring of the velocity does not alter the row-sums of the coefficient matrix $\boldsymbol{C}$. Consequently, the row-sums remain equal to two times the corresponding diagonal entry, and thus it is sufficient to have a zero at the diagonal. We define the value of an out-of-domain convective flux such that the corresponding diagonal entry of $\boldsymbol{C}$ is zero. For example, near the wall $y = 0$ the out-of-domain mass flux $\bar{\bar{u}}_{-1/2,j}$ follows from the requirement that the diagonal entry (3.31) equals zero. That is, for $i = 1$:

$$\begin{aligned} \bar{\bar{u}}_{i-3/2,j} := \quad & -3^{d+2} \quad (\bar{u}_{i+1/2,j} + \bar{v}_{i+1/2,j} - \bar{u}_{i-1/2,j} - \bar{v}_{i+1/2,j-1}) \\ & + \quad (\bar{\bar{u}}_{i+3/2,j} + \bar{\bar{v}}_{i+1/2,j+1} - \bar{\bar{v}}_{i+1/2,j-2}). \end{aligned}$$

In this way the boundary conditions are built into the coefficient matrices $\boldsymbol{M}$ and $\boldsymbol{C}$ without violating (3.26) and (3.20). Thus also for non-periodic conditions, the mass, momentum and kinetic energy are conserved if $\boldsymbol{D} = \mathbf{0}$.

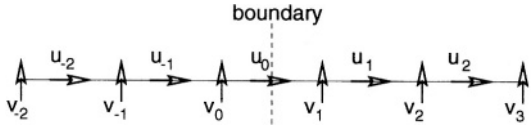

Figure 3.3. The location of the ghost velocities. Here, the velocity normal to the wall is denoted by u; v represents the tangential velocity. The discrete velocity u_0 lies at the wall. u_{-1}, u_{-2}, v_0 and v_{-1} are ghost velocities. The other discrete velocities lie in the fluid.

The diffusive fluxes through near-wall control faces are discretized such that the resulting coefficient matrix $\boldsymbol{D}$ is symmetric. The symmetry of $\boldsymbol{D}$ is preserved if the velocity-gradient is mirrored in a no-slip wall. We implement this condition by means of ghost velocities.

Figure 3.3 illustrates the positioning of the ghost velocities near a Dirichlet boundary $y = 0$. The velocity at the wall is given by (u_Γ, v_Γ). The grid is also mirrored in $y = 0$. The symmetry of the coefficient matrix $\boldsymbol{D}$ is unbroken if the near-boundary diffusive fluxes are computed with the help of

$$\begin{aligned} u_0 &= u_\Gamma & v_\Gamma - v_0 &= v_1 - v_\Gamma \\ u_\Gamma - u_{-1} &= u_1 - u_\Gamma & v_\Gamma - v_{-1} &= v_2 - v_\Gamma \\ u_\Gamma - u_{-2} &= u_2 - u_\Gamma & v_\Gamma - v_{-2} &= v_3 - v_\Gamma \end{aligned}$$

3. A test-case: turbulent channel flow

In this section, the symmetry-preserving discretization is tested for turbulent channel flow. The Reynolds number is set equal to Re = 5,600 (based on the channel width and the bulk velocity), a Reynolds number at which direct numerical simulations have been performed by several research groups; see [12]-[14]. In addition we can compare the numerical results to experimental data from Kreplin and Eckelmann [15].

As usual, the flow is assumed to be periodic in the stream- and span-wise direction. Consequently, the computational domain may be confined to a channel unit of dimension $2\pi \times 1 \times \pi$, where the width of the channel is normalized. All computations presented in this section have been performed with 64 (uniformly distributed) stream-wise grid points and 32 (uniformly distributed) span-wise points. In the lower-half of the channel, the wall-normal grid points are computed according to

$$y_j = \frac{\sinh(\gamma j/N_y)}{2\sinh(\gamma/2)} \qquad \text{with} \quad j = 0, 1, ..., N_y/2,$$

where N_y denotes the number of grid points in the wall-normal direction. The stretching parameter γ is taken equal to 6.5. The grid points in the upper-half are computed by means of symmetry.

The temporal integration of (3.1) is performed with the help of a one-leg method that is tuned to improve its convective stability [16]. The non-dimensional time step is set equal to $\delta t = 1.25\ 10^{-3}$. Mean values of computational results are obtained by averaging the results over the directions of periodicity, the two symmetrical halves of the channel, and over time. The averaging over time starts after a start-up period. The start-up period as well as the time-span over which the results are averaged, 1500 non-dimensional time-units, are identical for all the results shown is this section. Figure 3.4 shows

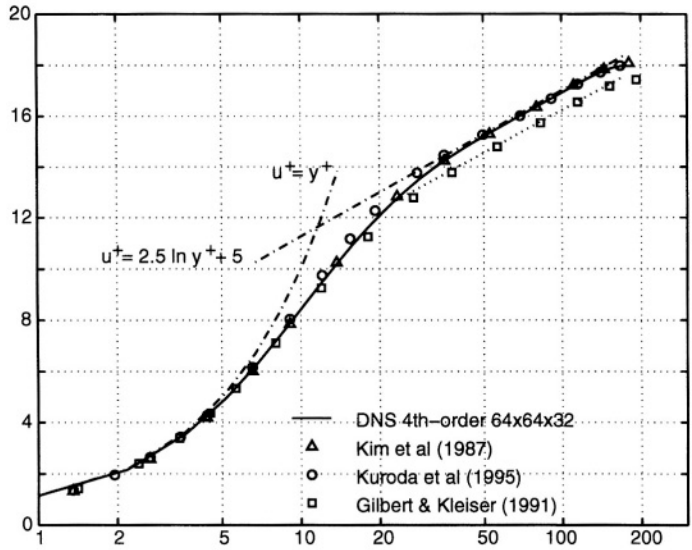

Figure 3.4. The mean stream-wise velocity u^+ versus y^+. The dashed lines represent the law of the wall and the log law. The markers represent DNS-results that are taken from the ERCOFTAC Database.

a comparison of the mean velocity profile as obtained from our fourth-order symmetry-preserving simulation ($N_y = 64$) with those of other direct numerical simulations. Here it may be stressed that the grids used by the DNS's that we compare with have typically about 128^3 grid points, that is 16 times more grid points than our grid has. Nevertheless, the agreement is excellent.

To investigate the convergence of the fourth-order method upon grid refinement, we have monitored the skin friction coefficient C_f as obtained from simulations on four different grids. We will denote these grids by A, B, C and D. Their spacings differ only in the direction normal to the wall. They have $N_y = 96$ (grid A), $N_y = 64$ (B), $N_y = 56$ (C) and $N_y = 48$ (D) points in the wall-normal direction, respectively. The first (counted from the wall) grid line used for the convergence study is located at $y_1^+ \approx 0.95$ (grid A), $y_1^+ \approx 1.4$ (B), $y_1^+ \approx 1.6$ (C), and $y_1^+ \approx 1.9$ (D), respectively. Figure 3.5 displays the skin friction coefficient C_f as function of the fourth power of y_1^+. The convergence study shows that the discretization scheme is indeed fourth-order accurate (on a non-uniform mesh). This indicates that the underlying physics is resolved when 48 or more grid points are used in the wall normal direction. In terms of the local grid spacing (measured by y_1^+), the skin friction coefficient is approximately given by $C_f = 0.00836 - 0.000004(y_1^+)^4$. The extrapolated value at $y_1^+ = 0$ lies in between the C_f reported by Kim *et al.* [12] and Dean's correlation of $C_f = 0.073\ Re^{-1/4} = 0.00844$ [17].

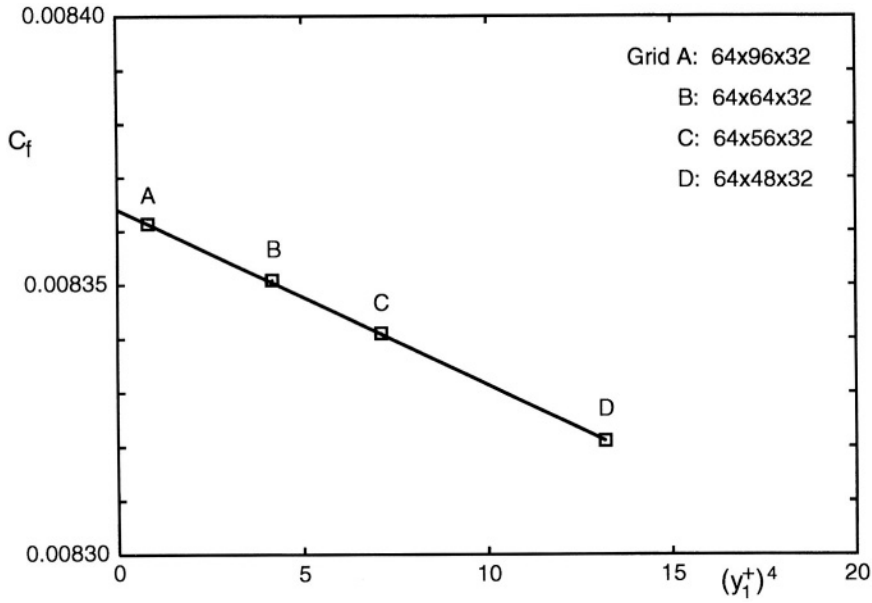

Figure 3.5. Convergence of the skin friction coefficient C_f upon grid refinement. The figure displays C_f versus the fourth power of the first grid point y_1^+.

The convergence of the fluctuating stream-wise velocity near the wall ($0 < y^+ < 20$) is presented in Figure 3.6. Here, we have added results obtained on three still coarser grids (with $N_y = 32$, $N_y = 24$ and $N_y = 16$ points in the wall-normal direction, respectively), since the results on the grids A, B, C and D fall almost on top of each other. The coarsest grid, with only $N_y = 16$ points to cover the channel width, is coarser than most of the grids used to perform a large-eddy simulation (LES) of this turbulent flow. Nevertheless, the $64 \times 16 \times 32$ solution is not that far off the solution on finer grids, in the near wall region. Further away from the wall, the turbulent fluctuations predicted on the coarse grids ($N_y \leq 32$) become too high compared to the fine grid solutions, as is shown in Figure 3.7.

The solution on the $64 \times 24 \times 32$, for example, forms an excellent starting point for a large-eddy simulation. The root-mean-square of the fluctuating stream-wise velocity is not far of the fine grid solution, and viewed through physical glasses, the energy of the resolved scales of motion, the coarse grid ($N_y = 24$) solution, is convected in a stable manner, because it is conserved by the discrete convective operator. Therefore, we think that the symmetry-preserving discretization forms a solid basis for testing sub-grid scale models. The discrete convective operator transports energy from a resolved scale of motion to other resolved scales without dissipating any energy, as it should do from a physical point of view. The test for a sub-grid scale model then

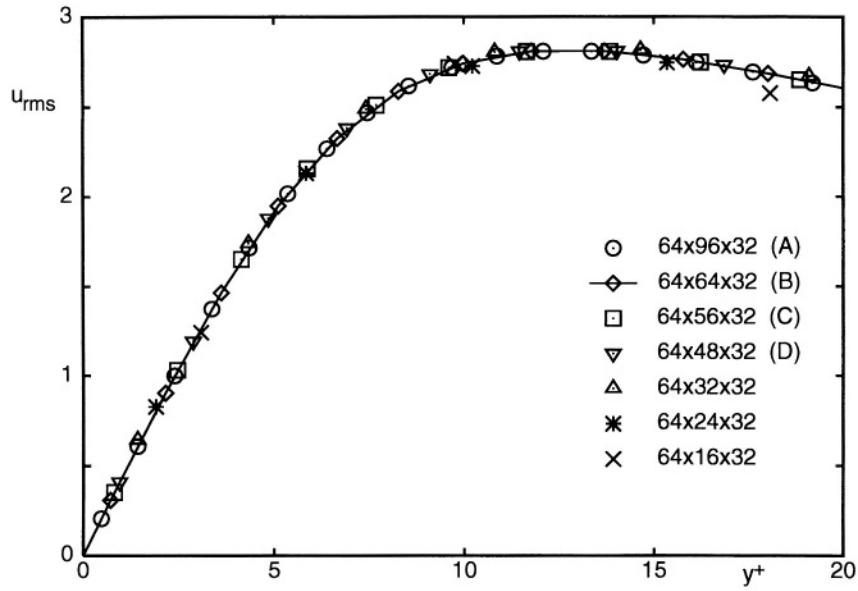

Figure 3.6. The root-mean-square velocity fluctuations normalized by the wall shear velocity as function of the wall coordinate y^+ on various grids for $y^+ \leq 20$. The markers correspond to the results obtained in the grid points. The solution on grid B is also represented by a continuous line.

reads: does the addition of the dissipative sub-grid model to the conservative convection of the resolved scales reduce the error in the computation of $u_{\rm rms}$.

The results for the fluctuating stream-wise velocity $u_{\rm rms}$ are compared to the experimental data of Kreplin and Eckelmann [15] and to the numerical data of Kim *et al.* [12] in Fig. 3.8. This comparison confirms that the fourth-order, symmetry-preserving method is more accurate than the second-order method. With 48 or more grid points in the wall normal direction, the root-mean-square of the fluctuating velocity obtained by the fourth-order method is in close agreement with that computed by Kim *et al.* [12] for $y^+ > 20$ (Figure 3.8 shows this only for y^+ up to 40; yet, the agreement is also excellent for $y^+ > 40$). In the vicinity of the wall ($y^+ < 20$), the velocity fluctuations of the fourth-order simulation method fit the experiment data nicely, even up to very coarse grids with only 24 grid points in the wall-normal direction. However, the turbulence intensity in the sub-layer ($0 < y^+ < 5$) predicted by the simulations is higher than that in the experiment. According to the fourth-order simulation the root-mean-square approaches the wall like $u_{\rm rms} \approx 0.38 y^+$ ($N_y = 64$). The exact value of this slope is hard to pin-point experimentally. Hanratty *et al.* [18] have fitted experimental data of several investigators, and thus came to 0.3. Most direct numerical simulations yield higher values. Kim *et al.* [12] and

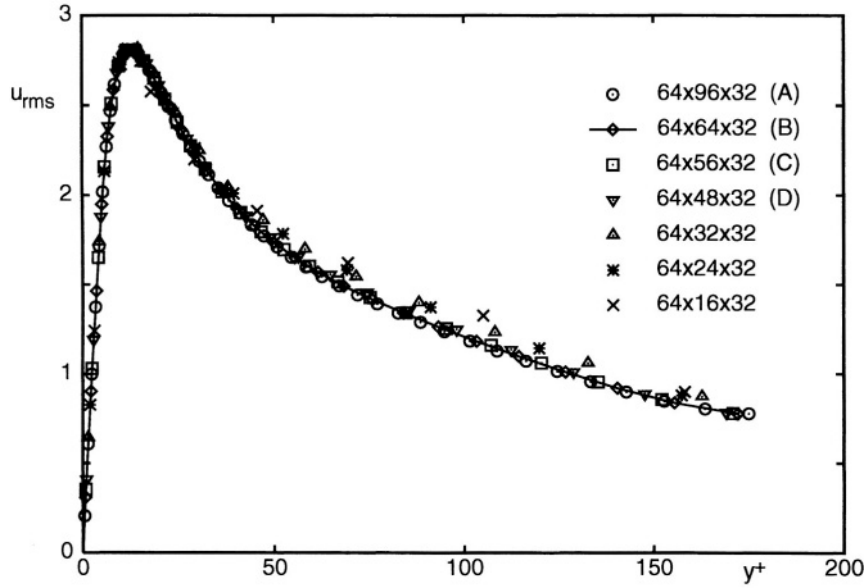

Figure 3.7. The root-mean-square velocity fluctuations normalized by the wall shear velocity for $y^+ \leq 200$ on various grids.

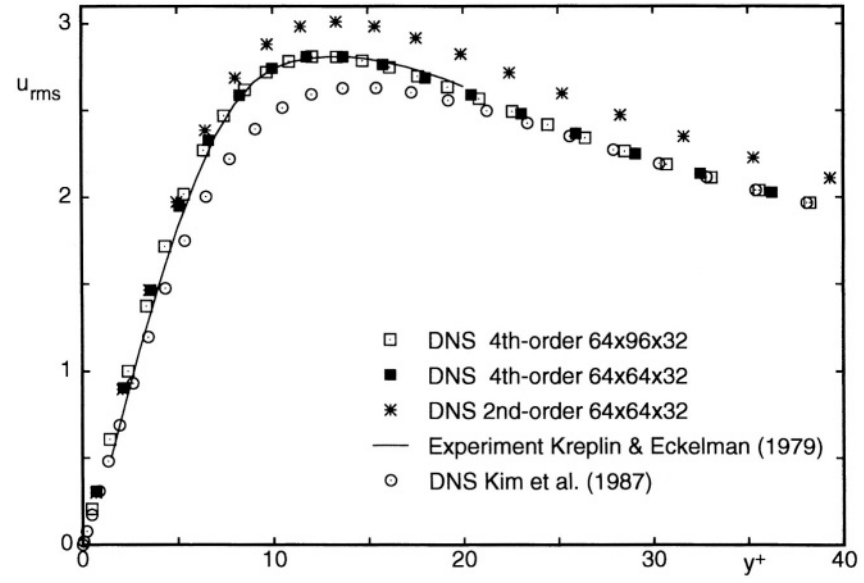

Figure 3.8. Comparison of the mean-square of the stream-wise fluctuating velocity as function of y^+.

Gilbert and Kleiser [13] have found slopes of 0.3637 and 0.3824 respectively, which is in close agreement with the present findings.

So, in conclusion, the results of the fourth-order symmetry-preserving discretization agree better with the available reference data than those of its second-order counterpart, and with the fourth-order method a $64 \times 64 \times 32$ grid suffices to perform an accurate DNS of a turbulent channel flow at Re=5,600.

4. Conclusions

The smallest scales of motion in a turbulent flow result from a subtle balance between convective transport and diffusive dissipation. In mathematical terms, the balance is an interplay between two differential operators differing in symmetry: the convective derivative is skew-symmetric, whereas diffusion is governed by a symmetric, positive-definite operator. With this in mind, we have developed a spatial discretization method which preserves the symmetries of the balancing differential operators. That is, convection is approximated by a skew-symmetric discrete operator, and diffusion is discretized by a symmetric, positive-definite operator. Second-order and fourth-order versions have been developed thus far, applicable to structured non-uniform grids. The resulting semi-discrete representation conserves mass, momentum and energy (in the absence of physical dissipation). As the coefficient matrices are stable and non-singular, a solution can be obtained on any grid, and we need not add an artificial damping mechanism that will inevitably interfere with the subtle balance between convection and diffusion at the smallest length scales. This forms our motivation to investigate symmetry-preserving discretizations for direct numerical simulation (DNS) of turbulent flow. Because stability is not an issue, the main question becomes how accurate is a symmetry-preserving discretization, or stated otherwise, how coarse may the grid be for a DNS? This question has been addressed for a turbulent channel flow. The outcomes show that with the fourth-order method a $64 \times 64 \times 32$ grid suffices to perform an accurate DNS of a turbulent channel flow at Re=5,600.

References

[1] R.W.C.P. Verstappen and A.E.P. Veldman, Spectro-consistent discretization of Navier-Stokes: a challenge to RANS and LES, *J. Engng. Math.* **34**, 163 (1998).

[2] Y. Morinishi, T.S. Lund, O.V. Vasilyev and P. Moin, Fully conservative higher order finite difference schemes for incompressible flow, *J. Comp. Phys.* **143**, 90 (1998).

[3] O.V. Vasilyev, High order finite difference schemes on non-uniform meshes with good conservation properties. *J. Comp. Phys.* **157**, 746

(2000).

[4] F. Ducros, F. Laporte, T. Soulères, V. Guinot, P. Moinat and B. Caruelle, High-order fluxes for conservative skew-symmetric-like schemes in structured meshes: application to compressible flows. *J. Comp. Phys.* **161**, 114 (2000).

[5] A. Twerda, A.E.P. Veldman and S.W. de Leeuw, High order schemes for colocated grids: Preliminary results. In: *Proc. 5th annual conference of the Advanced School for Computing and Imaging* 286 (1999).

[6] A. Twerda, Advanced computational methods for complex flow simulation. Delft University of Technology, PhD thesis (2000).

[7] J.M. Hyman, R.J. Knapp and J.C. Scovel, High order finite volume approximations of differential operators on nonuniform grids, *Physica D* **60**, 112 (1992).

[8] T.A. Manteufel and A.B. White, Jr., The numerical solution of second-order boundary value problems on nonuniform meshes, *Math, of Comp.* **47**, 511 (1986).

[9] A.E.P. Veldman and K. Rinzema, Playing with nonuniform grids, *J. Engng. Math* **26**, 119 (1991).

[10] F.H. Harlow and J.E. Welsh, Numerical calculation of time-dependent viscous incompressible flow of fluid with free surface, *Phys. Fluids* **8**, 2182 (1965).

[11] M. Antonopoulos-Domis, Large-eddy simulation of a passive scalar in isotropic turbulence, *J. Fluid Mech.* **104**, 55 (1981).

[12] J. Kim, P. Moin and R. Moser, Turbulence statistics in fully developed channel flow at low Reynolds number, *J. Fluid Mech.* **177**, 133 (1987).

[13] N. Gilbert and L. Kleiser, Turbulence model testing with the aid of direct numerical simulation results, in *Proc. Turb. Shear Flows 8,* Paper 26-1, Munich (1991).

[14] A. Kuroda, N. Kasagi and M. Hirata, Direct numerical simulation of turbulent plane Couette-Poisseuille flows: effect of mean shear rate on the near-wall turbulence structures, in: *Proc Turb. Shear Flows 9,* F. Durst *et al.* (eds.), Berlin: Springer-Verlag 241-257 (1995).

[15] H.P. Kreplin and H. Eckelmann, Behavior of the three fluctuating velocity components in the wall region of a turbulent channel flow, *Phys Fluids* **22**, 1233 (1979).

[16] R.W.C.P. Verstappen and A.E.P. Veldman, Direct numerical simulation of turbulence at lower costs, *J. Engng. Math.* **32**, 143 (1997).

[17] R.B. Dean, Reynolds number dependence of skin friction and other bulk flow variables in two-dimensional rectangular duct flow, *J. Fluids. Engng.* **100**, 215 (1978).

[18] T.J. Hanratty, L.G. Chorn and D.T. Hatziavramidis, Turbulent fluctuations in the viscous wall region for Newtonian and drag reducing fluids, *Phys Fluids* **20**, S112 (1977). *Int. J. Heat Mass Transfer* **24**, 1541 (1981).